NAVAL AIR WARFARE CENTER AIRCRAFT DIVISION
PATUXENT RIVER, MARYLAND

TECHNICAL REPORT

REPORT NO: NAWCADPAX/TR-2012/206

STRESS CORROSION CRACKING OF ALUMINUM ALLOYS

by

E. U. Lee
R. Taylor
C. Lei
B. Pregger
E. Lipnickas

10 September 2012

DEPARTMENT OF THE NAVY
NAVAL AIR WARFARE CENTER AIRCRAFT DIVISION
PATUXENT RIVER, MARYLAND

NAWCADPAX/TR-2012/206
10 September 2012

STRESS CORROSION CRACKING OF ALUMINUM ALLOYS

by

E. U. Lee
R. Taylor
C. Lei
B. Pregger
E. Lipnickas

RELEASED BY:

10 Sep 2012

KEVIN J. KOVALESKI / AIR-4.3.4 / DATE
Head, Materials Engineering Division
Naval Air Warfare Center Aircraft Division

REPORT DOCUMENTATION PAGE

Form Approved
OMB No. 0704-0188

1. REPORT DATE	2. REPORT TYPE	3. DATES COVERED
10 September 2012	Technical Report	

4. TITLE AND SUBTITLE	5a. CONTRACT NUMBER
Stress Corrosion Cracking of Aluminum Alloys	5b. GRANT NUMBER
	5c. PROGRAM ELEMENT NUMBER

6. AUTHOR(S)	5d. PROJECT NUMBER
E. U. Lee R. Taylor C. Lei B. Pregger E. Lipnickas	5e. TASK NUMBER
	5f. WORK UNIT NUMBER

7. PERFORMING ORGANIZATION NAME(S) AND ADDRESS(ES)	8. PERFORMING ORGANIZATION REPORT NUMBER
Naval Air Warfare Center Aircraft Division 48066 Shaw Road , Unit 5 Patuxent River, Maryland 20670-1908	NAWCADPAX/TR-2012/206

9. SPONSORING/MONITORING AGENCY NAME(S) AND ADDRESS(ES)	10. SPONSOR/MONITOR'S ACRONYM(S)
Naval Air Systems Command 47123 Buse Road Unit IPT Patuxent River, Maryland 20670-1547	11. SPONSOR/MONITOR'S REPORT NUMBER(S)

12. DISTRIBUTION/AVAILABILITY STATEMENT

Approved for public release; distribution is unlimited.

13. SUPPLEMENTARY NOTES

14. ABSTRACT

The effects of environment concentration and strain rate on the stress corrosion cracking (SCC) behavior of 5083-H131 and 7075-T6 aluminum alloys were studied, conducting electrochemical measurement and slow strain rate test. The employed environments were pH 7.3 aqueous solutions of 0 to 20% NaCl, and the applied strain rate ranged from 10^{-8} s^{-1} to 10^{-4} s^{-1}. A comparative test was also carried out in air. After the tests, the fracture surface morphology was examined by scanning electron microscopy, and the microstructure in the vicinity of the fracture by light microscopy to clarify the SCC mode. The results indicated: 1. The SCC susceptibility is a little below 0.5% NaCl but it is raised noticeably with increasing NaCl concentration above 0.5% NaCl. 2. Compared to 7075-T6 aluminum alloy, 5083-H131 aluminum alloy has inferior mechanical property and it is highly susceptible to SCC. 3. The corrosion potential is lower and the corrosion rate is greater for higher NaCl concentration. 4. The SCC susceptibility increases with decreasing strain rate. 4. The SCC mode is crack initiation at the junctions of grain boundaries with specimen surface, and crack propagation along grain boundaries into the specimen, attributed to hydrogen embrittlement and anodic dissolution.

15. SUBJECT TERMS

Stress Corrosion Cracking (SCC); 5083-H131; 7075-T6; Slow Strain Rate Test (SSRT)

16. SECURITY CLASSIFICATION OF:			17. LIMITATION OF ABSTRACT	18. NUMBER OF PAGES	19a. NAME OF RESPONSIBLE PERSON
a. REPORT	b. ABSTRACT	c. THIS PAGE			19b. TELEPHONE NUMBER (include area code)
Unclassified	Unclassified	Unclassified	SAR	36	Eun Lee (301) 342-8069

Standard Form 298 (Rev. 8-98)
Prescribed by ANSI Std. Z39-18

SUMMARY

The effects of environment concentration and strain rate on the stress corrosion cracking (SCC) behavior of 5083-H131 and 7075-T6 aluminum alloys were studied, conducting electrochemical measurement and slow strain rate test. The employed environments were pH 7.3 aqueous solutions of 0 to 20% NaCl, and the applied strain rate ranged from 10^{-8} s^{-1} to 10^{-4} s^{-1}. A comparative test was also carried out in air. After the tests, the fracture surface morphology was examined by scanning electron microscopy, and the microstructure in the vicinity of the fracture by light microscopy to clarify the SCC mode. The results indicated: 1. The SCC susceptibility is a little below 0.5% NaCl but it is raised noticeably with increasing NaCl concentration above 0.5% NaCl. 2. Compared to 7075-T6 aluminum alloy, 5083-H131 aluminum alloy has inferior mechanical property and it is highly susceptible to SCC. 3. The corrosion potential is lower and the corrosion rate is greater for higher NaCl concentration. 4. The SCC susceptibility increases with decreasing strain rate. 4. The SCC mode is crack initiation at the junctions of grain boundaries with specimen surface, and crack propagation along grain boundaries into the specimen, attributed to hydrogen embrittlement and anodic dissolution.

Contents

ACKNOWLEDGMENT

This study was supported by the Office of Naval Research, Reference No. N0001412AF00002. Special thanks are due to Drs. R. Williams and A. K. Vasudevan and Mr. W. C. Nickerson of ONR for monitoring this study and providing technical guidance.

INTRODUCTION

During 1960s, two accelerated Stress Corrosion Cracking (SCC) test techniques, based on different mechanical approaches, emerged. One technique tests statically loaded precracked specimens and analyzes the test-result, using linear elastic fracture mechanics. Its advantage is the easy determination of the crack growth rate and the threshold stress intensity for SCC from the test result. The other conducts Slow Stain Rate Test (SSRT) on smooth or precracked specimens. This test has been carried out to investigate the SCC behavior of steels by Kim [1] and Saxena[2], define the effect of environment concentration and applied potential on SCC by Roychowhury,[3] determine the influence of environment, oxidizing condition, temperature and strain rate on SCC by Payer,[4] examine the mechanistic aspects of SCC in aluminum alloys by Watkinson[5] and Scamans,[6] evaluate the differences in SCC susceptibility of different aluminum alloys, including 7075-T6, by Brown,[7] Buhl[8] and Ugiansky,[9] study the SCC resistance of 5083 aluminum alloy by Czechowski[10] and Al-Li alloy by Braun[11], clarify the synergistic effect of acidic pH and elevated temperature on the SCC of marternsitic stainless steel by Roy,[12] and learn the annealing effect on SCC of carbon steel by Haruna.[13] The application of slow straining frequently facilitates cracking in circumstances where, at constant load or constant total strain, cracking is not observed, shows poor reproducibility, or takes a long time.[14] Therefore, the SSRT is much more effective in producing SCC than the static test, and the incubation period for crack nucleation and the testing time are considerably reduced. The SSRT is applicable to the evaluation of a wide variety of metallic materials in test environments which simulate aqueous, nonaqueous, and gaseous service environments over a wide range of temperatures and pressures that may cause SCC of susceptible materials.

The most significant variable in SSRT is the strain rate. It has been reported that the SSRT does not produce SCC at either extreme of strain rates but will produce SCC in a critical range of strain rates characteristic of each material.[8,14] Below the minimum strain rate, corrosion may be prevented due to oxide film repair so that the necessary reaction of bare metal cannot be sustained, and SCC may not occur. On the one hand, above the maximum strain rate, ductile failure by void coalescence would occur because of insufficient time for the electrochemical reaction, associated with SCC. The other variable in SSRT is the aggressiveness of environment. The susceptibility to SCC was observed to be higher with greater concentration of corrosive environment.[3,15]

On the one hand, the electrochemical potential and current measurements during SCC and other localized corrosion processes have also been useful in defining and understanding the SCC mechanism, and have been used to elucidate the cracking behavior in many metal-environment systems.[3,16-18]

This study was conducted to clarify the role of corrosive environment concentration, strain rate, and electrochemical parameters, playing in the SCC of two aluminum alloys, 5083-H131 and 7075-T6.

EXPERIMENTAL PROCEDURE

SPECIMENS

As the specimen materials, 5083-H131 and 7075-T6 aluminum alloys were selected. Their nominal compositions are shown in Table 1. The 5083-H131 aluminum alloy was sensitized at 175^{o}C for 240 hr in air. Figure A-1 shows the optical micrographs of the as-polished specimens of the two alloys. From these alloys, smooth, round tension test specimens, having a gage section 38.1 mm (1.5 in.) long by 6.35 mm (0.25 in.) diameter, were machined in S-L orientation. Those specimens were subjected to mechanical testing and SSRT.

Table 1: Chemical Compositions of 5083 and 7075 Aluminum Alloys (Weight Percent)

	Cu	Mn	Mg	Cr	Zn	Fe	Si	Ti	Al
5083	0.10	0.4-1.0	4.0-4.9	0.05-0.25	0.25	0.40	0.40	0.15	bal
7075	1.2-2.0	0.30	2.1-2.9	0.18-0.40	5.1-6.1	0.7	0.5	0.2	bal

ELECTROCHEMICAL MEASUREMENTS

Sheet specimens of 76.2 x 76.2 x 4.8 mm (3 x 3 x 3/16 in.) were machined from the two aluminum alloys, 5083-H131 and 7075-T6, for the electrochemical measurement. Subsequently, they were polished at one side to 800 grit (10 micron) SiC paper.

The electrochemical polarization experiment was conducted with a Solartron electrochemical measuring system, consisting of an SI 1260 impedance/gain-phase analyzer and a SI 1287 electrochemical interface, in pH 7.3 aqueous quiescent solutions of 0.001 to 20% NaCl concentrations. The polarization curves were performed after a “dwell” time of 10 min to determine corrosion potential at a sweep rate of 0.1667 mVs^{-1} from 15 mV below the corrosion potential to 15 mV above. From the polarization curve, the corrosion potential and corrosion current density were obtained, and the corrosion rate was calculated using the following equation.[19]

$$CR = K_1.(i_{corr} / \rho).EW \qquad \text{Eq. (1)}$$

where

CR = corrosion rate, mm/yr
K_1 = constant, 3.27 x 10^{-3} mm g/μA cm yr
i_{corr} = corrosion current density, μA/cm^2
ρ = density, g/cm^3
EW = alloy equivalent weight

SLOW STRAIN RATE TEST

The SSRT was conducted in an apparatus, consisting of a specimen-cell, a reservoir of NaCl solution and a pump. The NaCl solution was circulated between the specimen-cell and the reservoir by the pump during the SSRT. The gage section of the specimen was totally immersed in the NaCl solution during the test. The specimens were pulled in tension to fracture at strain rates, ranging from 10^{-8} to 10^{-4} s^{-1}. The test environments were pH 7.3 aqueous solutions of 0 to 20% NaCl concentrations at ambient temperature. Comparative tests were also conducted in air. In the analysis of test results, the fracture strength, time, and strain were taken as the measures of SCC susceptibility, and their variation with NaCl concentration and strain rate was evaluated. (Other investigators[14] employed maximum load, elongation, reduction of area or fracture energy as the measure of SCC susceptibility, in addition to fracture strength and time.)

After the test, the fracture surface morphology was examined with a JEOL* SEM JSM- 6460LV scanning electron microscope, operated at an accelerating voltage of 20 kV, and the microstructure near the fracture with a Nikon Epiphot 300 optical microscope (Nikon Instruments Inc., Tokyo, Japan). (*JEOL is a trademark of Japan Electron Optics Ltd., Tokyo.)

RESULTS

The results include those of mechanical testing, electrochemical measurement and SSRT.

MECHANICAL PROPERTIES

The mechanical properties of 5083-H131 and 7075-T6 in S-L orientation are shown in Table 2.

Table 2: Mechanical Properties of 5083-H131 and 7075-T6 Aluminum Alloys in S-L Orientation

	UTS MPa (ksi)	US MPa (ksi)	Harness (Rockwell B)	Elongation
5083-H131	310 (45)	193 (28)	39	9.2
7075-T6	538 (78)	469 (68)	88	9.5

Compared to the 7075-T6, the 5083-H131 has a lower ultimate tensile strength, a lower yield strengths, a lower hardness, but a similar elongation.

POLARIZATION MEASUREMENT

The polarization curves from the electrochemical measurement are shown for the two aluminum alloys in NaCl solutions of different concentrations in Figure A-2. The corrosion potentials E_{corr}, corrosion current densities i_{corr}, and calculated corrosion rates CR are shown in Table 3. Furthermore, the variations of corrosion potential and corrosion rate with NaCl concentration are shown in Figures A-3(a) and (b), respectively.

Table 3: Polarization Test Result for 5083-H131 and 7075-T6 Aluminum Alloys

NaC1 Concentration (%)	Corrosion Potential, E_{corr} (V)		Corrosion Current Density, i_{corr} ($\mu A/cm^{2)}$		Corrosion Rate, CR (mm/yr)	
	5083	7075	5083	7075	5083	7075
0.001	-0.60	-0.62	3.35E-06	2.45E-06	9.50E-04	1.03E-04
0.005	-0.66	-0.65	1.04E-05	2.35E-06	2.95E-03	8.20E-05
0.5	-0.72	-0.72	4.08E-05	3.40E-05	1.16E-02	1.9E-03
3.5	-0.78	-0.77	2.10E-04	4.14E-04	5.97E-02	1.45E-02
10.0	-0.81	-0.82	4.86E-04	3.50E-04	1.38E-01	1.22E-02
20.0	-0.84	-.085	2.07E-04	5.58E-04	5.87E-02	1.95E-02

Higher NaCl concentration moves the corrosion potential E_{corr} to active (or lower) direction almost equally, thus enhancing hydrogen generation and corrosion, in both of the aluminum alloys, Table 3 and Figure A-3(a). The corrosion rate CR, increasing with increasing NaCl concentration, is higher in 5083-H131 than in 7075-T6 within the range of NaCl concentration employed, Table 3 and Figure A-3(b).

SSRT RESULTS

Figures A-4(a) and (b) show the variation of fracture strength and time with NaCl concentration at strain rate 10^{-7} s^{-1}. These plots indicate:

- For the NaCl concentration below 0.5%, the fracture strength and time are nearly constant, but above 0.5% they decrease noticeably with increasing NaCl concentration.
- This result indicates that the SCC susceptibility is low and nearly constant below 0.5% NaCl concentration, whereas it is noticeably raised with increasing NaCl concentration above 0.5%.
- Compared to those for the 7075-T6, the fracture strength and time for the 5083-H131 are much lower, evidencing the greater susceptibility of 5083-H131 to SCC.

Figures A-5(a) and (b) show the variation of fracture strength and time with strain rate in air and 3.5% NaCl solution. These plots indicate:

- In air, the fracture strength is reduced little and the fracture time is extended with decreasing strain rate.
- In 3.5% NaCl solution, the decrease in fracture strength and the increase in fracture time are substantial with decreasing strain rate, especially at strain rates below 10^{-6} s^{-1}.
- The fracture strength is less in 3.5% NaCl than in air for a given strain rate. [The difference is attributable to the environment assisted cracking, SCC, in 3.5% NaCl solution.]
- For a given strain rate, the fracture strength is much lower and the fracture time is shorter for the 5083-H131 than for the 7075-T6 in 3.5% NaCl solution. [This observation evidences that the SCC susceptibility is greater for the 5083-H131 than for the 7075-T6.]

Figure A-6 shows the variation of fracture strain (or strain to fracture) with strain rate in air and 3.5% NaCl solution. The variation features are similar to those for the fracture strength, shown in Figure A-5(a).

Figure A-7 shows the SEM fractographs of 5083-H131 specimens, tested at strain rate of 10^{-7} s^{-1} in aqueous solutions of 0.035 and 10% NaCl. The following is observable.

- After testing in 0.035% NaCl solution, the fracture surface consists of smooth faces of elongated grains and patches of dimples. The former (smooth faces of elongated grains) presumably resulted from intergranular separation by SCC, and the latter (dimple patches) from overload fracture. In other words, the specimen fracture under slow straining in 0.035% NaCl solution is attributable to a combination of partial SCC and partial overload fracture.

- After testing in 10% NaCl solution, the low magnification fractograph shows faintly a flat smooth circular band along the periphery. Its higher magnification fractograph shows elongated flat grains, some flaking along the boundaries. This observation evidences the interganular SCC.

Figure A-8 shows micrographs of a plane normal to the fracture surface of the 5083-H131 specimen, tested at strain rate of 10^{-7} s^{-1} in 20% NaCl solution. Under slow straining in 20% NaCl solution, cracks were initiated from multiple sites on the side face of the specimen and grown along grain boundaries into the specimen, and finally the specimen was fractured apart. In the fracture surface (top of the micrograph), flaking of elongated grains along their boundaries is also observable. This observation confirms the interganular SCC.

Figure A-9 shows the SEM fractographs of the 7075-T6 specimens, which were subjected to SSRT in air and 20% NaCl solution, respectively. The two sets of fractographs show that:

- The fracture surface of the specimen tested in air shows dimples with neither slow crack growth area nor corroded area, typical of overload or mechanical fracture in non-corrosive environment.

- The fracture surface of the specimen tested in 20% NaCl solution consists of a relatively flat and smooth circular band along the periphery and a coarse center portion. The SEM fractograph of the former shows corrosion product covering the fracture surface, indicating environment assisted subcritical crack growth. That of the latter shows dimples with no corrosion product, typical of overload or mechanical fracture.

Figure A-10 shows the optical micrographs of a plane normal to the fracture surface of the 7075-T6 specimen tested at strain rate 10^{-7} s^{-1} in 20% NaCl solution. The top line indicates the flat and smooth portion of the fracture surface along the boundaries of grains elongated in the L-orientation. The two side-lines indicate the side faces of the specimen along the S-orientation. It is observable that several cracks were emanated from the both side faces and propagated perpendicularly to the axial loading direction, branching along grain boundaries, into the

specimen. This observation evidences a subcritical intergranular stress corrosion crack growth, initiated from multiple nucleation sites on the cylindrical side face of the specimen. The crack initiation sites are found to be the junctions of grain boundaries with the side face of the specimen, as shown in the micrographs.

DISCUSSION

SCC SUSCEPTIBILITY INDEX

As Figure A-5(a) shows, the fracture strength is less in NaCl solution than in air, noticeable more at a lower strain rate. The fracture strength reduction must be attributed to SCC in the NaCl solution, and the value normalized with the fracture strength in air can be a representative measure of SCC susceptibility. Therefore, a SCC susceptibility index, I_{stress}, is defined as:

$$I_{stress} = \Delta\sigma / \sigma_{air} \qquad \text{Eq. (2)}$$

where:

$\Delta\sigma = \sigma_{air} - \sigma_{NaCl}$
σ_{air} = fracture strength in air
σ_{NaCl} = fracture strength in NaCl solution

As Figures A-7 and A-9 show, the fracture surface of the specimen, subjected to SSRT in NaCl solution, consists of areas of SCC and mechanical (or overload) fracture. The SCC area normalized with the area of mechanical fracture can be another measure of SCC susceptibility. Therefore, second SCC susceptibility index, I_{area}, is defined as.

$$I_{area} = A_{scc} / A_{mech} \qquad \text{Eq. (3)}$$

where:

A_{scc} = area of SCC in fracture surface
A_{mech} = area of mechanical (or overload) fracture in fracture surface

The variations of these indexes with strain rate and NaCl concentration are shown in Figures A-11 and A-12. Figure A-11 indicates that the first SCC susceptibility index, I_{stress}, is greater for the 5083-H131 than for the 7075-T6 at a given strain rate. Figure A-12 indicates that the second SCC susceptibility index, I_{area}, is also greater for the 5083-H131 than for the 7075-T6 at a given strain rate and a given NaCl concentration. Furthermore, the variation of these indexes also shows that the SCC susceptibilities of the two aluminum alloys are greater for lower strain rate and higher NaCl concentration.

Combining Figures A-3(b) and A-12(b), both of the corrosion rate and SCC index are plotted together against the NaCl concentration for the 5083-H131 and 7075-T6 in Figures A-13(a) and (b). The features of the corrosion rate increase with NaCl concentration in the absence of

straining are similar to those of the SCC index increase with NaCl concentration under slow straining for both of the alloys. This observation demonstrates that a greater corrosion rate in the absence of straining results in a greater SCC susceptibility under slow straining.

ENVIRONMENT CONCENTRATION AND SCC SUSCEPTIBILITY

It was observed that the SCC susceptibility of the two aluminum alloys is low and nearly constant in aqueous solutions of NaCl concentration less than 0.5%, as shown in Figures A-4 and A-12(b). Other investigators also made similar observations. In his study on SCC of AISI 304 stainless steel, Roychowdhury[3] detected no apparent SCC in solutions containing 1 ppm thiosulfate and gradual SCC with increasing thiosulfate concentration. Trabanelli[15] found no evidence of SCC of AISI 304 stainless steel in 10^{-5} M NaF solution but intergranular SCC by increasing the NaF concentration. Micheli[21] noticed solution-treated AISI 316L stainless steels immune to SCC in aqueous NaCl solutions up to 3 mol/L.

STRAIN RATE AND SCC SUSCEPTIBILITY

From Figure A-5(a), it is clear that the 5083-H131 and 7075-T651 aluminum alloys are not susceptible to SCC in air under straining at rates, 10^{-7} – 10^{-4} s^{-1}. This observation agrees with some other investigators. Parkins reported no detectable SCC in soft mild steel under straining at rates, 10^{-5} – 10^{-2} s^{-1}, in air.[22] Henry Holroyd and Scamans observed no SCC occurring in 5083 H115 aluminum alloy at strain rates, 10^{-4} - 10^{-3} s^{-1}, in air.[23] Yu et al found 70/30 brass unsusceptible to SCC in air.[24]

As shown in Figures A-5, A-6, A-11, and A-12(a), in corrosive environments, the SCC susceptibility, indicated by fracture strength, time and strain, and SCC index, keeps increasing with decreasing strain rate from 10^{-4} to 10^{-8} s^{-1}. Similar observations were also made by some investigators.[22-24] Parkins[22] found the SCC susceptibility of mild steel in 1M NaH_2PO_4 at -1 V (SCE) increasing with decreasing strain rate from 10^{-2} to 10^{-6} s^{-1}. Yu et al[24] found the SCC susceptibility of 70/30 brass in 1M $NaNO_2$ increasing with decreasing strain rate from 10^{-3} to 10^{-7} s^{-1}. Holroyd[23] noticed the SCC susceptibility of 5050A wire in 3% NaCl + 0.3% H_2O_2 solution increasing with decreasing strain rate from 10^{-3} to 10^{-6} s^{-1}. However, the other investigators[1,8,9,14,25] reported that the SCC susceptibility, indicated by maximum load, area reduction, elongation or fracture energy, decreased after reaching the maximum at a strain rate, 10^{-5} s^{-1}, 10^{-6} s^{-1} or 10^{-7} s^{-1}.

It has been understood that the surfaces of aluminum alloys tend to be covered with oxide film in corrosive environment. On the SCC susceptibility change with strain rate, it was suggested that at high strain rates, the corrosion process cannot keep up with the staining process, and the influence of corrosion is negligible.[8] With decreasing strain rate, the latter influence becomes more significant. The attack by the corrosive environment reaches a maximum at a strain rate where the repassivation or oxide film formation can overtake the activation caused by the straining. The formation of oxide film on a metal surface reduces the reactivity of the underlying metal, and its rupture must occur before a crack can be initiated. According to the film-rupture theory, rupture takes place during straining by slip-steps emerging at the surface, and localized

corrosion and/or anodic dissolution then occurs at the small area of freshly exposed metal to initiate a crack.[1] On the other hand, during a static test, there is no way of sustaining the rate of slip-step emergence other than by increasing the applied stress or strain – that is, in a static load test, the driving force for slip relaxes with time. However, when dynamic strain is applied in the slow strain test, slip-step emergence is induced artificially at a relatively constant rate which ensures film rupture. At further decreasing strain rate below its minimum, active sites are repassivated or filmed with oxide before a corrosion attack can take place. This results in a reduction of SCC susceptibility. However, the absence of such a strain-rate-minimum in this study may be attributable to very slow or incomplete repassivation at the applied minimum strain rate 10^{-8} s^{-1} in the specimens of 5083-H131 and 7075-T6 aluminum alloys under the employed test condition.

SCC MECHANISM

The SCC susceptibility of aluminum alloys depends on metallurgical treatment and microstructure. The SCC attack is usually intergranular and involves the presence of an active constituent in the grain boundaries. On the other hand, embrittlement of grain boundary by hydrogen, adsorbed and/or generated by grain boundary and crack tip local cell corrosion reaction, has also been known to play an important role in SCC. There have been several mechanisms proposed, capable of explaining the SCC behavior of aluminum alloys. Those mechanisms include, but not limited to, anodic dissolution[26-31] and hydrogen embrittlement[32-37] of grain boundary.

Precipitates are observable on the grain boundaries in both of the as-received alloys, Figure A-1. Those precipitates are reported to be Mg_2Al_3 in the 5083-H131[26] and $Cr_2Mg_3Al_{18}$ and $(Fe,Mn)Al_6$ in the 7075-T6.[38] Under slow straining in an aqueous NaCl solution, such a precipitate becomes anodic to the alloy matrix and dissolves, leading to the observed intergranular cracking and exemplifying the grain boundary anodic dissolution mechanism.[26-31] This is verified by the optical micrographs, Figures A-8 and A-10, in which fewer or no precipitates are observable in the vicinity of intergranular cracks of specimens, tested under slow straining in 20% NaCl solution.

As shown in Table 3 and Figure A-3(a), a higher NaCl concentration moves the corrosion potential down to more active direction or induces generation of a greater amount of hydrogen at the specimen surface exposed to aqueous NaCl solution. The hydrogen is believed to diffuse into grain boundaries more readily than into alloy matrix through the junctions of grain boundaries and specimen surface, and induces intergranular cracking. This is an example of grain boundary hydrogen embrittlement mechanism.[32-37] Therefore, the SCC mechanism for the two aluminum alloys must be simultaneous anodic dissolution and hydrogen embrittlement of grain boundaries under slow straining in an aqueous NaCl solution.

CONCLUSIONS

Compared to 7075-T6, 5083-H131 had inferior mechanical strength (UTS, YS, and hardness) in air and greater SCC susceptibility in NaCl solution.

Crack was initiated at the junctions of grain boundaries with the specimen surface and grown inward along grain boundaries under slow straining in a NaCl solution.

The SCC mechanism is simultaneous anodic dissolution and hydrogen embrittlement of grain boundaries.

THIS PAGE INTENTIONALLY LEFT BLANK

REFERENCES

1. C. D. Kim and R. F. Wilde: in *The Slow Strain Rate Technique*, G. M. Ugiansky and J. H. Payer, eds., ASTM STP 665, ASTM, Philadelphia, PA, 1979, pp. 97-112.

2. A. Saxena, R. K. Singh Raman and B. C. Muddle: *International Journal of Pressure Vessels and Piping*, 2006, Vol. 83, pp. 399-404.

3. S. Roychowdhury, S. K. Ghosal and P. K. De: *Journal of Materials Engineering and Performance*, 2004, Vol. 13(5), pp. 575-82.

4. J. H. Payer, W. E. Berry and R. N. Parkins: in *Stress Corrosion Cracking – The Slow Strain Rate Technique*, ASTM STP 665, G. M. Ugiansky and J. H. Payer, eds., ASTM, Philadelphia, PA, 1979, pp. 222-34.

5. F. E. Watkinson and J. C. Scully: *Corrosion Science*, 1972, Vol. 12, pp. 905-24.

6. G. M. Scamans, R. Alani and P. R. Swann: *Corrosion Science*, 1976, Vol. 16, pp. 443-59.

7. A. R. G. Brown and J. S. Gray: A Comparison of RAE Stress Corrosion Test Data on Aluminum Alloys, Including the Merits of the Testing Techniques, *Test Report 74153*, Royal Aircraft Establishment.

8. Buhl: in *Stress Corrosion Cracking – The Slow Strain Rate Technique*, G. M/ Ugiansky and J. H. Payer, eds., ASTM STP 665, ASTM, Philadelphia, PA, 1979, pp. 333-46.

9 G. M. Ugiansky, C. E. Johnson, D. S. Thompson and E. H. Gillespie: in *Stress Corrosion Cracking – The Slow Strain-Rate Technique*, ASTM STP 665, G. M. Ugiansky and J. H. Payer, eds., ASTM, Philadelphia, PA, 1979, pp. 254-65.

10 M. Czechowski: *Journal of Achievements in Materials and Manufacturing Engineering*, 2007, Vol. 20, Issues 11-2, pp. 219-22.

11. R. Braun: *Materials Science and Engineering*, 1995, Vol. A190, pp. 143-54.

12. A. K. Roy, M. K, Hossain and B. J, O'Toole: *Stress Corrosion Cracking of Martensitic Stainless Steel for Transmutation Application*, Presented at *2003 International High-Level Radioactive Waste Management Conference*, Las Vegas, Nevada, of 25 Nov 2002, Subject Category 2.8, Track No. 69425.

13. T. Haruna, L. Zhu and T. Shibata: *Corrosion Engineering*, 2000, Vol. 49, No. 3, pp. 138-43.

14. R. N. Parkins: in *The Slow Strain Rate Technique*, M. Ugiansky and J. H. Payer, eds., ASTM, STP 665, ASTM Philadelphia, PA, 1979, pp. 5-25.

15. G. Trabanelli, F. Zucchi and D. Demertzis: in *10th International Congress on Metallic Corrosion,* of 7-11 Nov 1987, Madras, India, 1987, Vol. 3, pp. 1905-12.

16. H. S. Issacs: *J. Electrochem. Soc.*, 1988, Vol. 135, pp. 2180-2183.

17. R. C. Newman, K. Sieradzki, and J. Woodward: *Corrosion Chemistry, Pits, Crevies and Cracks,* A. Turnbull, Ed., HMSO, 1987, p. 203.

18. A. Contreras, A. Albiter, M. Salazar, and R. Perez: *Materials Science and Engineering,* 2005, Vol. A 407, pp. 45-52.

19. ASTM G 102 – 89 (Reapproved 2004), "Standard Practice for Calculation of Corrosion Rates and Related Information from Electrochemical Measurements"

20. L. Raymond: *To be Published*

21. Lorenzo De Micheli, Silvia Maria Leite Agostinho, Giodano Trabanelli, Fabrizio Zucchi: Mat. Res., 2002, Vol. 5, No.1, pp.63-69.

22. R. N. Parkins: in *Environment-Sensitive Fracture: Evaluation and Comparison of Test Methods,* ASTM STP 821, S. W. Dean, E. N. Pugh, and G. M. Ugiansky, Eds., ASTM, Philadelphia, PA, 1984, pp. 5-31.

23. N. J. Henry Holroyd and G. M. Scamans: in *Environment-Sensitive Fracture: Evaluation and Comparison of Test Methods,* ASTM STP 821, S. W. Dean, E. N. Pugh, and G. M. Ugiansky, Eds., ASTM, Philadelphia, PA, 1984, pp. 202-241.

24. J. Yu, N. J. Henry Holroyd, and R. N. Parkins: in *Environment-Sensitive Fracture: Evaluation and Comparison of Test Methods,* ASTM STP 821, S. W. Dean, E. N. Pugh, and G. M. Ugiansky, Eds., ASTM, Philadelphia, PA, 1984, pp. 288-309.

25. M. Khobaib and C. T. Lynch: in *Environment-Sensitive Fracture: Evaluation and Comparison of Test Methods,* ASTM STP 821, S. W. Dean, E. N. Pugh, and G. M. Ugiansky, Eds., ASTM, Philadelphia, PA, 1984, pp. 242-255.

26. J. Gao: *PhD Thesis,* "Experiments to Explore the Mechanisms of Stress Corrosion Cracking," University of Rochester, Rochester, New York, 2011.

27. J. Gao and D. J. Quesnel: *Metall. Mater. Trans. A,* 2011, Vol. 42A, pp. 356-364.

28. J. Gao and D. J. Quesnel: *NACE International CORROSION 2010 Conference,* Paper No. 10303, San Antonio, TX, 2010.

29. J. L. Searles, P. I. Gouma, and R. G. Buchheit; *Metall. Mater. Trans. A,* 2001, Vol. 32, pp. 2859-2867.

30. J. L. Searles, P. I. Gouma, and R. G. Buchheit: *Mater. Sci. Forum*, 2002, Vol. 396-402, pp. 1437-1442.

31. R. G. Buchheit, R. K. Boger, M. C. Carroll, R. M. Leard, C. Paglia, and J. L. Searles: *JOM-J. Min. Met. Mat. S.,* 2001, Vol. 53, pp. 29-36.

32. R. J. Gest and A. R. Troiano: *Corrosion*, 1974, Vol. 30, pp. 274-279.

33. J. Albrecht, B. J. McTieman, I. M. Bernstein, and A. W. Thompson: *Scripta Metall.*, 1977, Vol. 11, pp. 893-897.

34. L. Christodoulou and H. M. Flower: *Acta Metall.*, 1980, Vol. 28, pp. 481-487.

35. D. A. Hardwick, A. W. Thompson, and I. M. Bernstein: *Corros. Sct.* 1988, Vol. 28, pp. 1127-1137.

36. R. H. Jones: *JOM-J. Min. Met. Mat. S.,* 2003, Vol. 55, pp. 42-46.

37. R. Song, W. Dietzel, B. J. Zhang, W. J. Liu, M. K. Tseng, and A. Atrens: *Acta Mater.*, 2004, Vol. 52, pp. 4727-4743.

38. *Metals Handbook*, Vol. 7, *Atlas of Microstructures of Industrial Alloys*, 8th Edition, American Society for Metals, Metals Park, OH, pp. 251. 1972.

THIS PAGE INTENTIONALLY LEFT BLANK

APPENDIX A
FIGURES

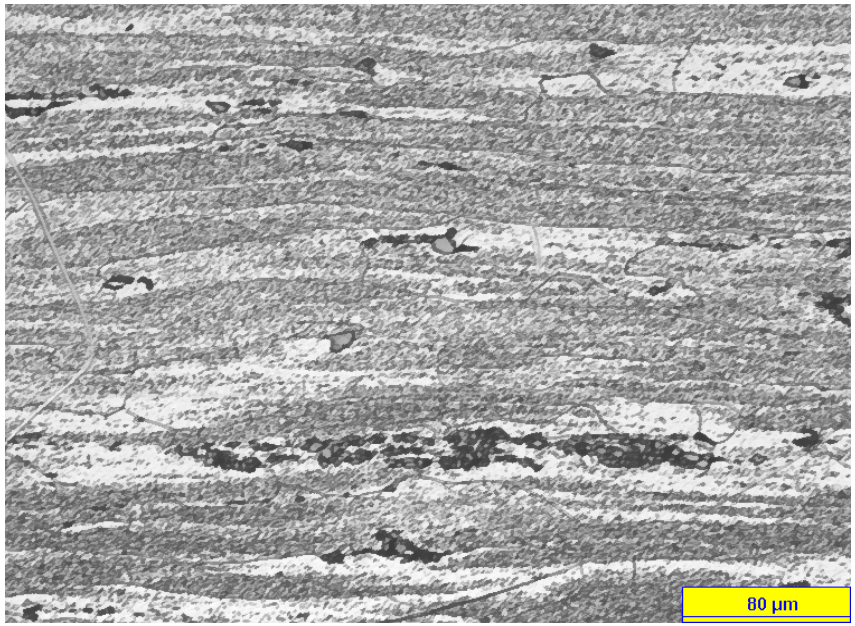

5083-H131

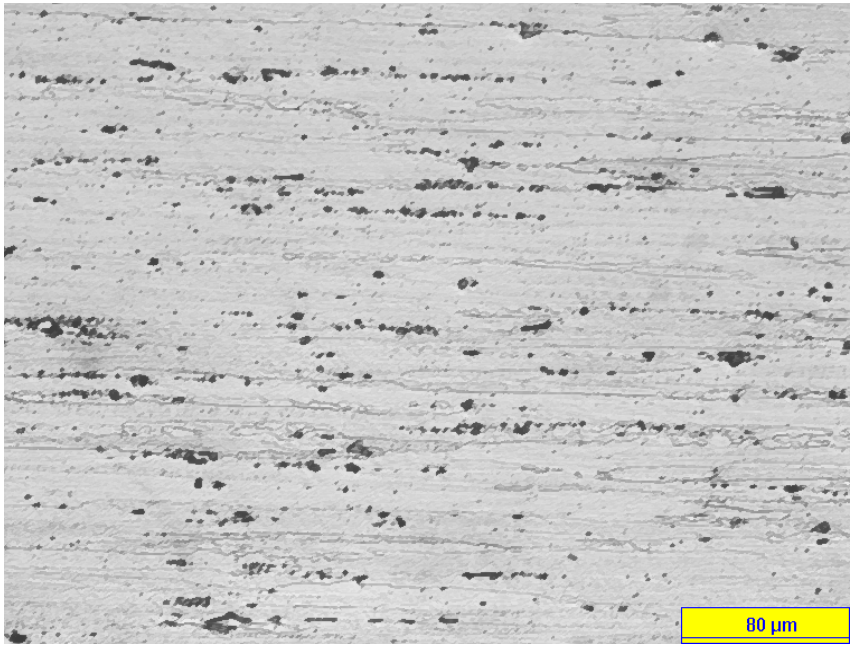

7075-T6

Figure A-1: Microstructures of 5083-H131 and 7075-T6 Aluminum Alloys

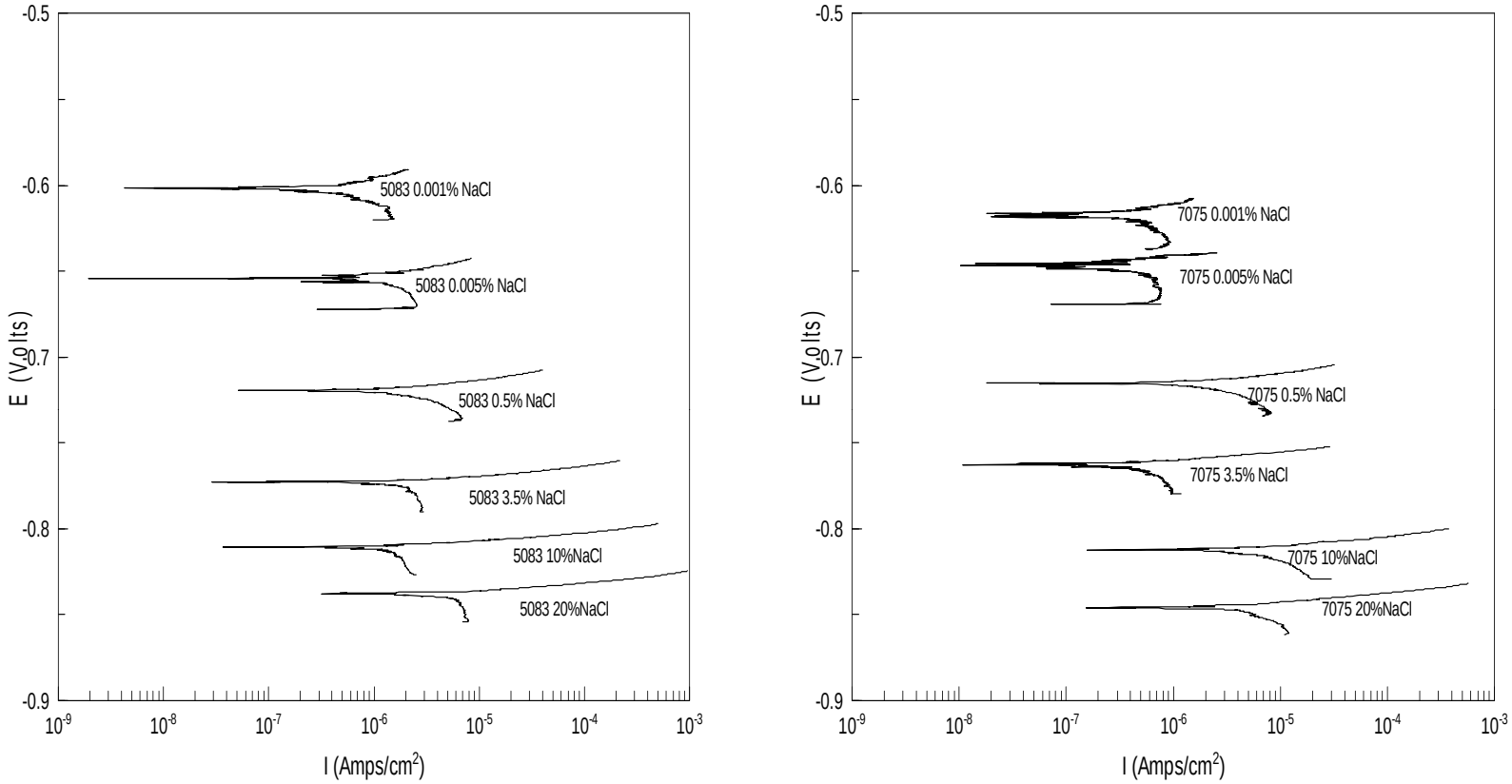

Figure A-2: Polarization Curves for 5083-H131 and 7075-T6 Aliminum Alloys in Aqueous Solutions of Different NaCl Concentrations

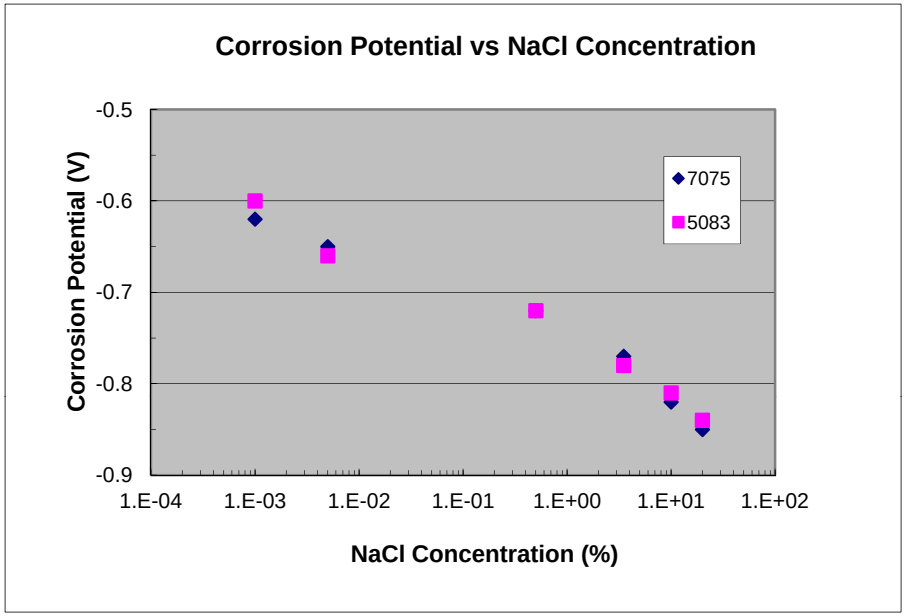

(a)

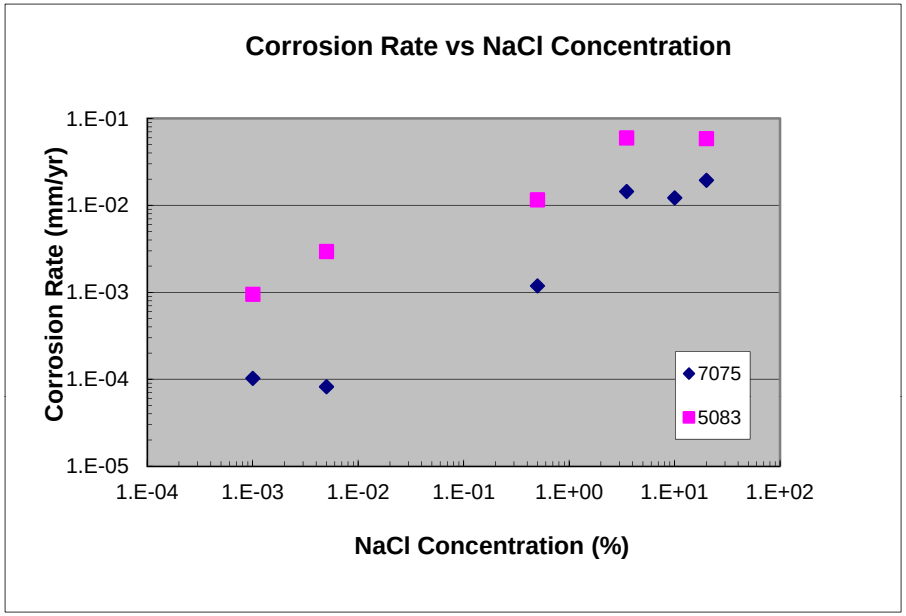

(b)

Figure A-3: Variation of Corrosion Potential and Corrosion Rate with NaCl Concentration

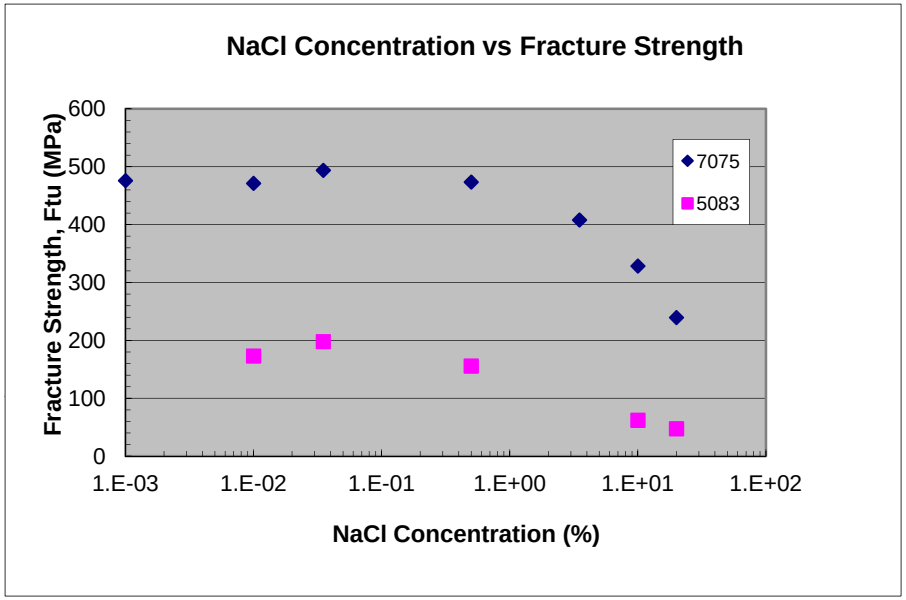

(a)

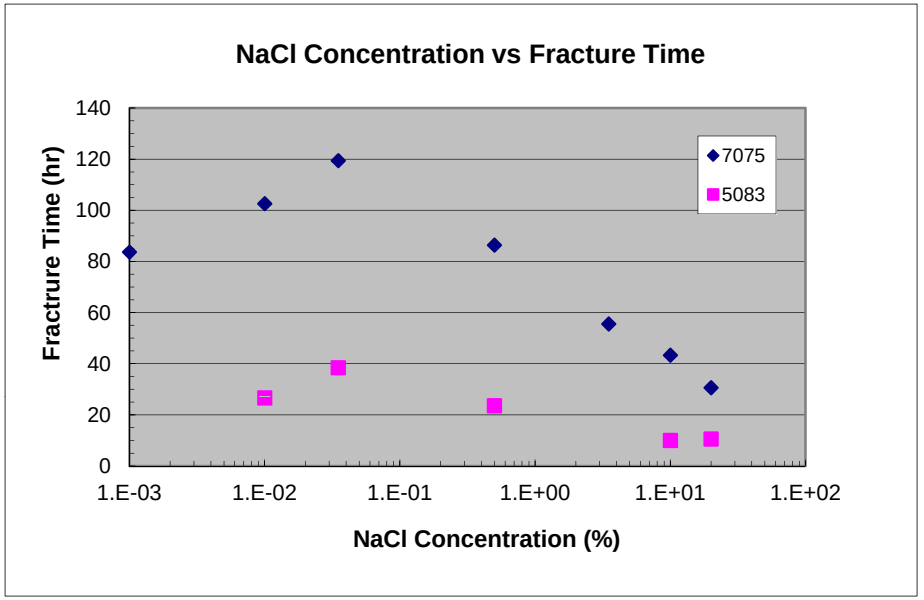

(b)

Figure A-4: Variation of Fracture Strength and Time with NaCl Concentration at Strain Rate 10^{-7} s^{-1}

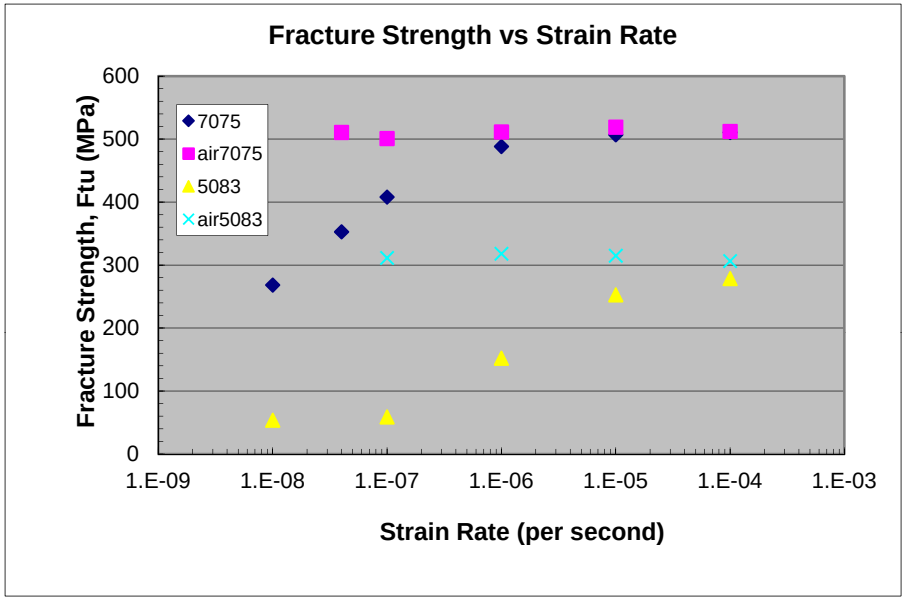

(a)

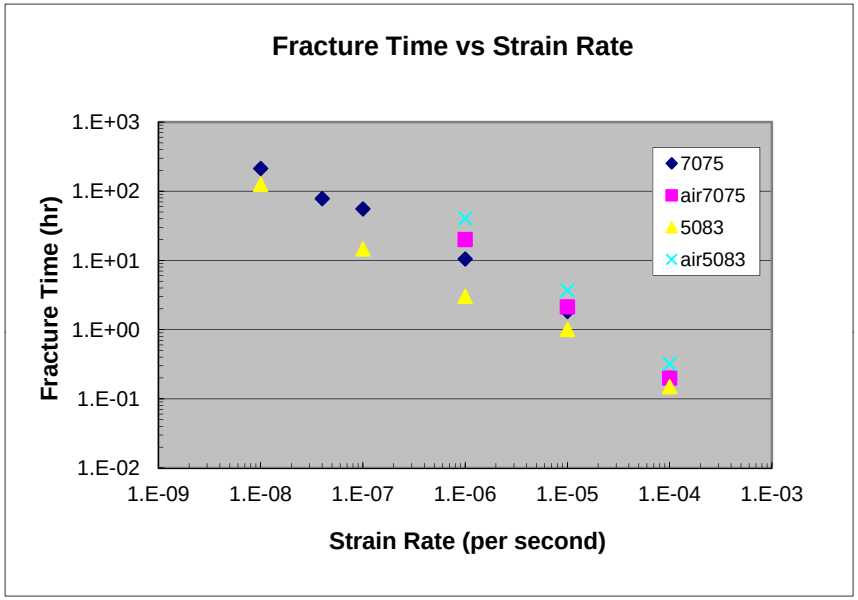

(b)

Figure A-5: Variation of Fracture Strength and Time with Strain Rate in Air and 3.5% NaCl Solution

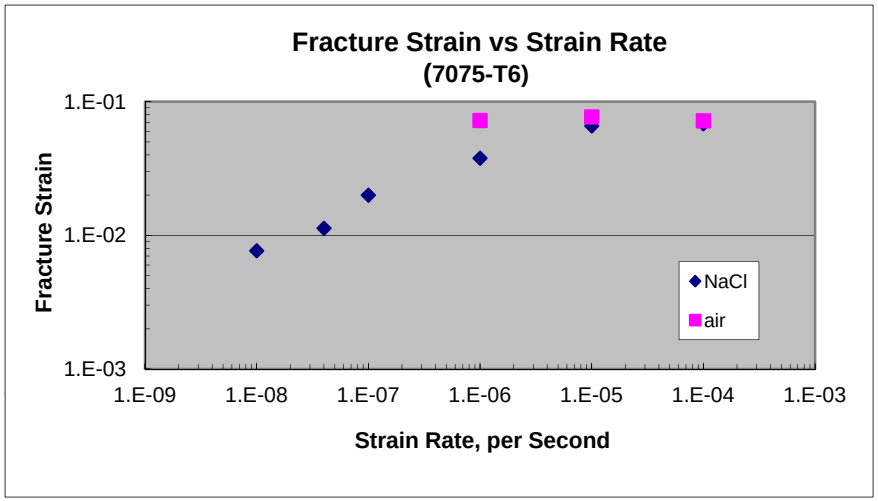

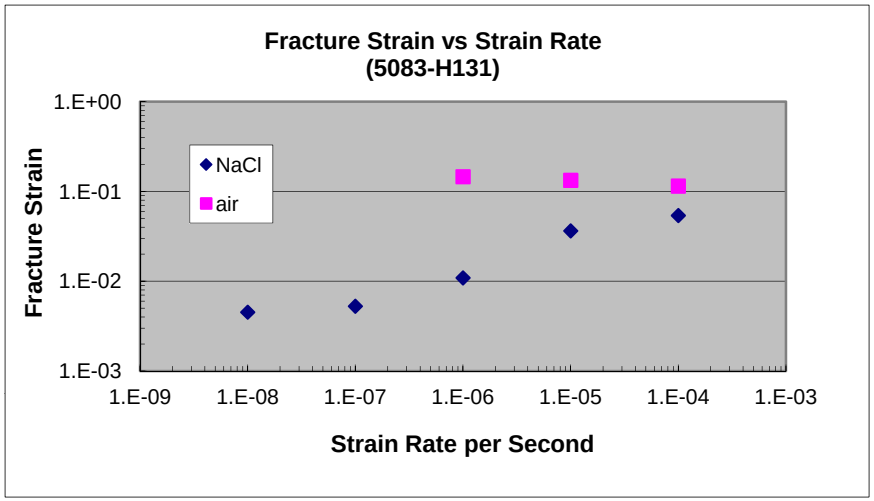

Figure A-6: Variation of Fracture Strain with Strain Rate in Air and 3.5% NaCl Solution

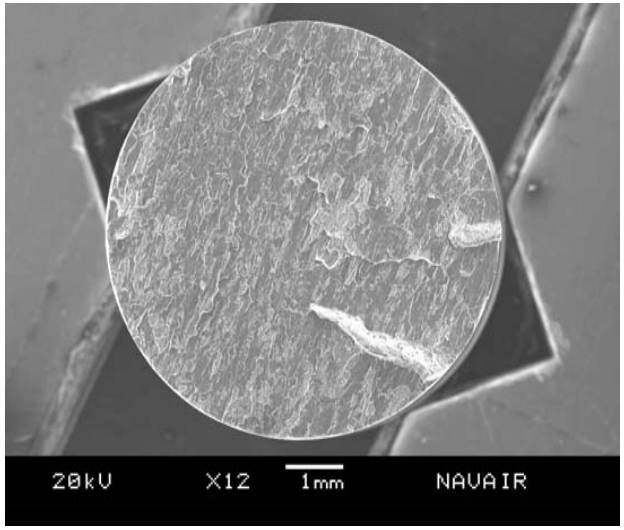

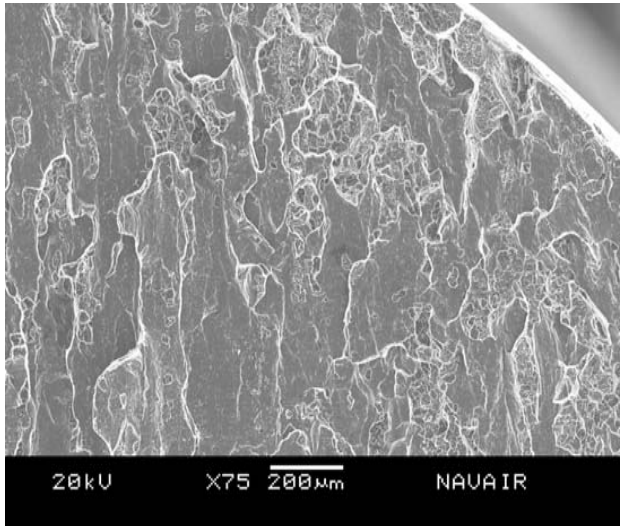

(Strain Rate 10^{-7} s^{-1} in 0.035% NaCl)

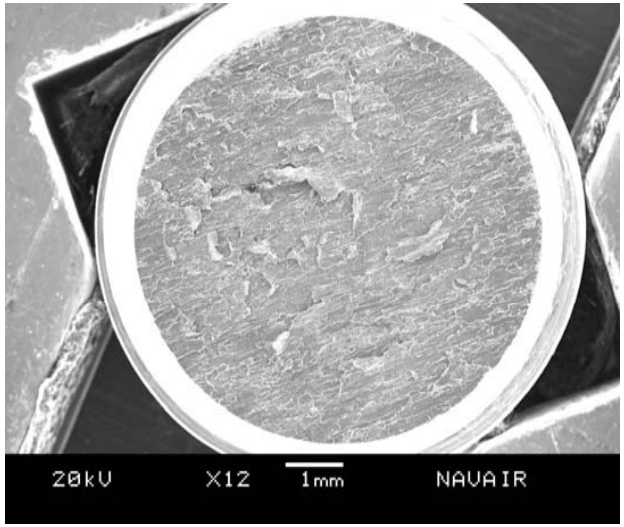

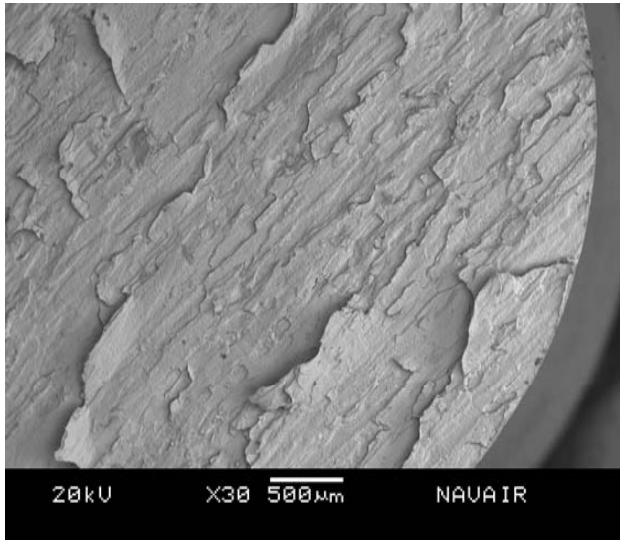

(Strain Rate 10^{-7} s^{-1} in 10% NaCl)

Figure A-7: SEM Fractographs of 5083-H131 Specimens, Tested at Strain Rate 10^{-7} s^{-1} in 0.035 and 10% NaCl Solutions

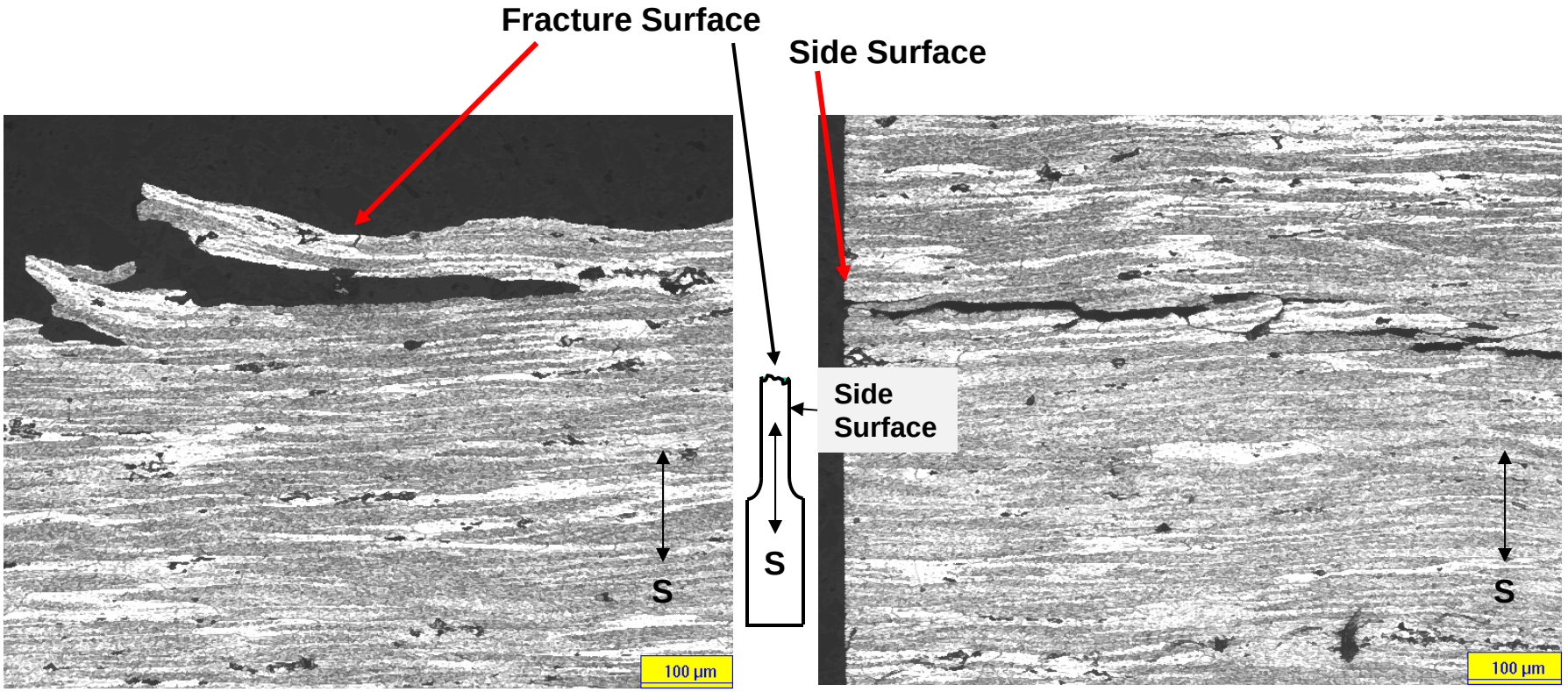

Figure A-8: Micrographs of a Plane Normal to Fracture Surface of 5083-H131 Specimen, Tested at Strain Rate 10^{-7} s^{-1} in 20% NaCl Solution

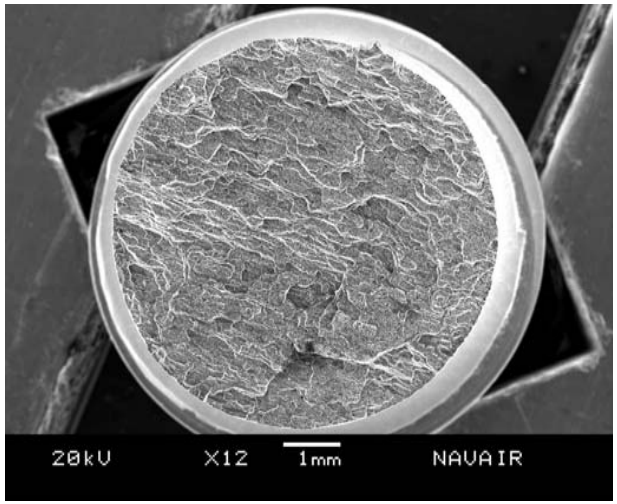

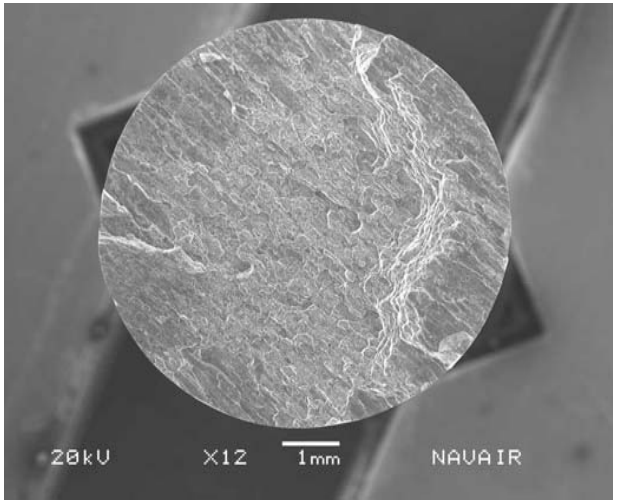

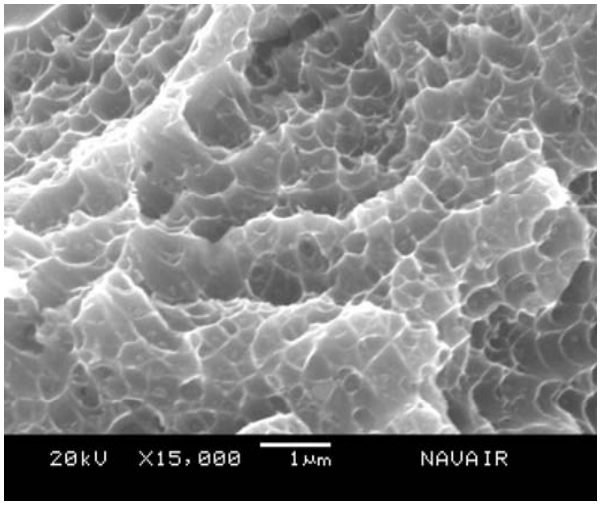

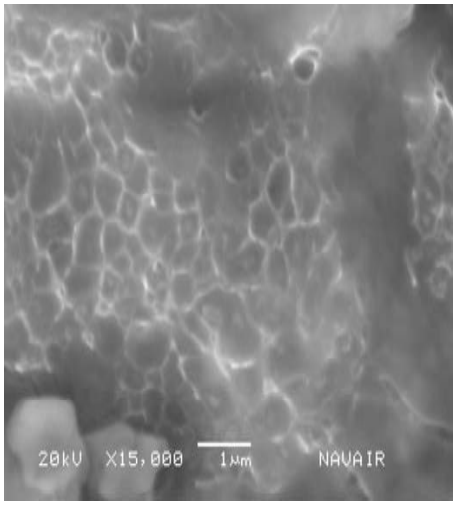

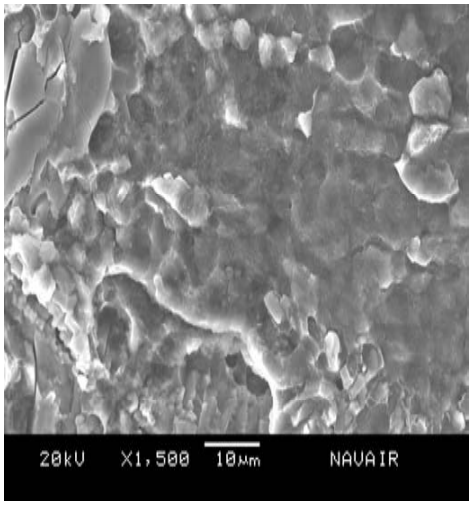

Center Portion Flat Smooth Band

(Strain Rate 10^{-4} s^{-1} in Air) (Strain Rate 10^{-7} s^{-1} in 20% NaCl)

Figure A-9: SEM Fractographs of 7075-T6 Specimens, Slow Strain Rate Tested in Air and 20% NaCl Solution

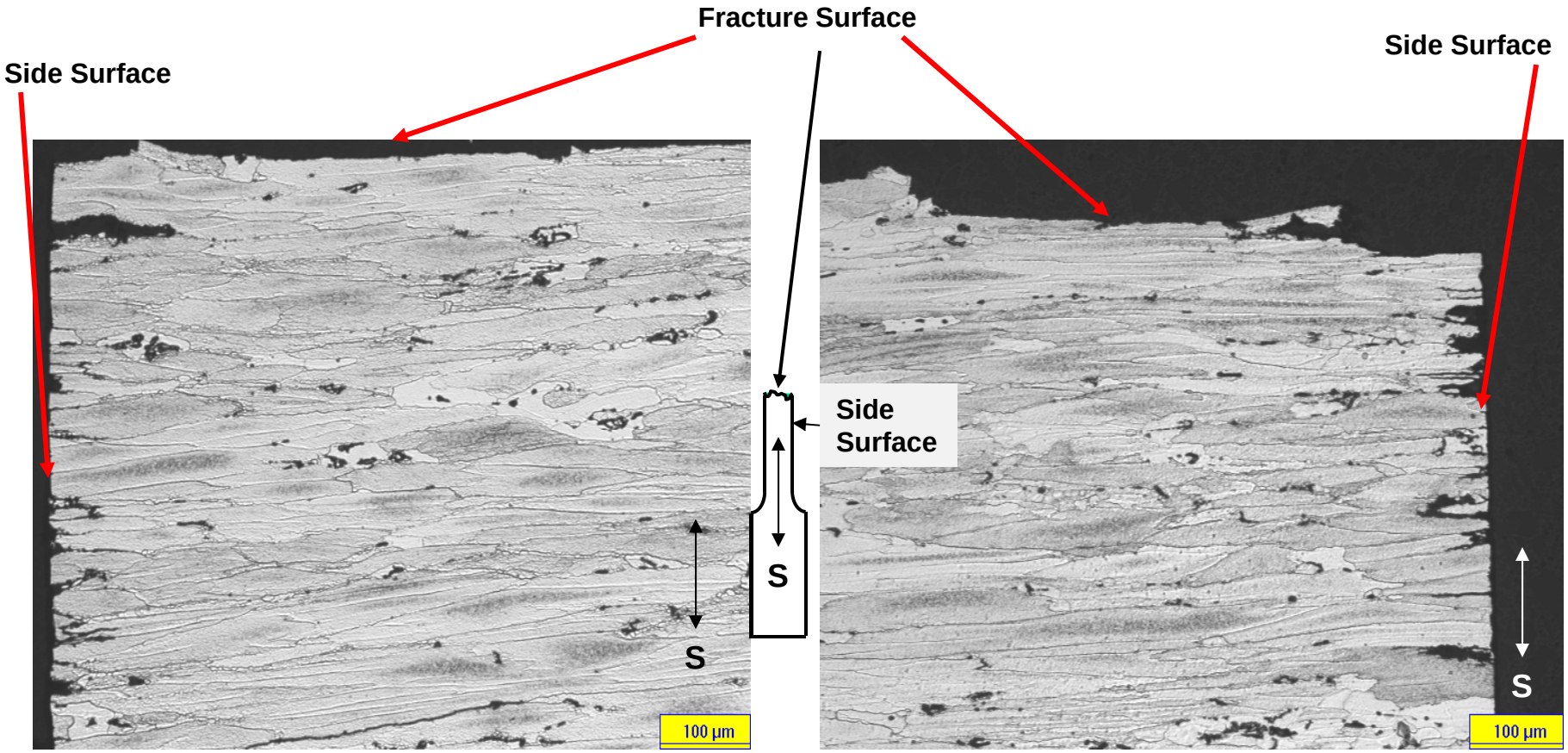

Figure A-10: Micrographs of a Plane Normal to Fracture Surface of 7075-T6 Specimen, Tested at Strain Rate 10^{-7} s^{-1} in 20% NaCl Solution

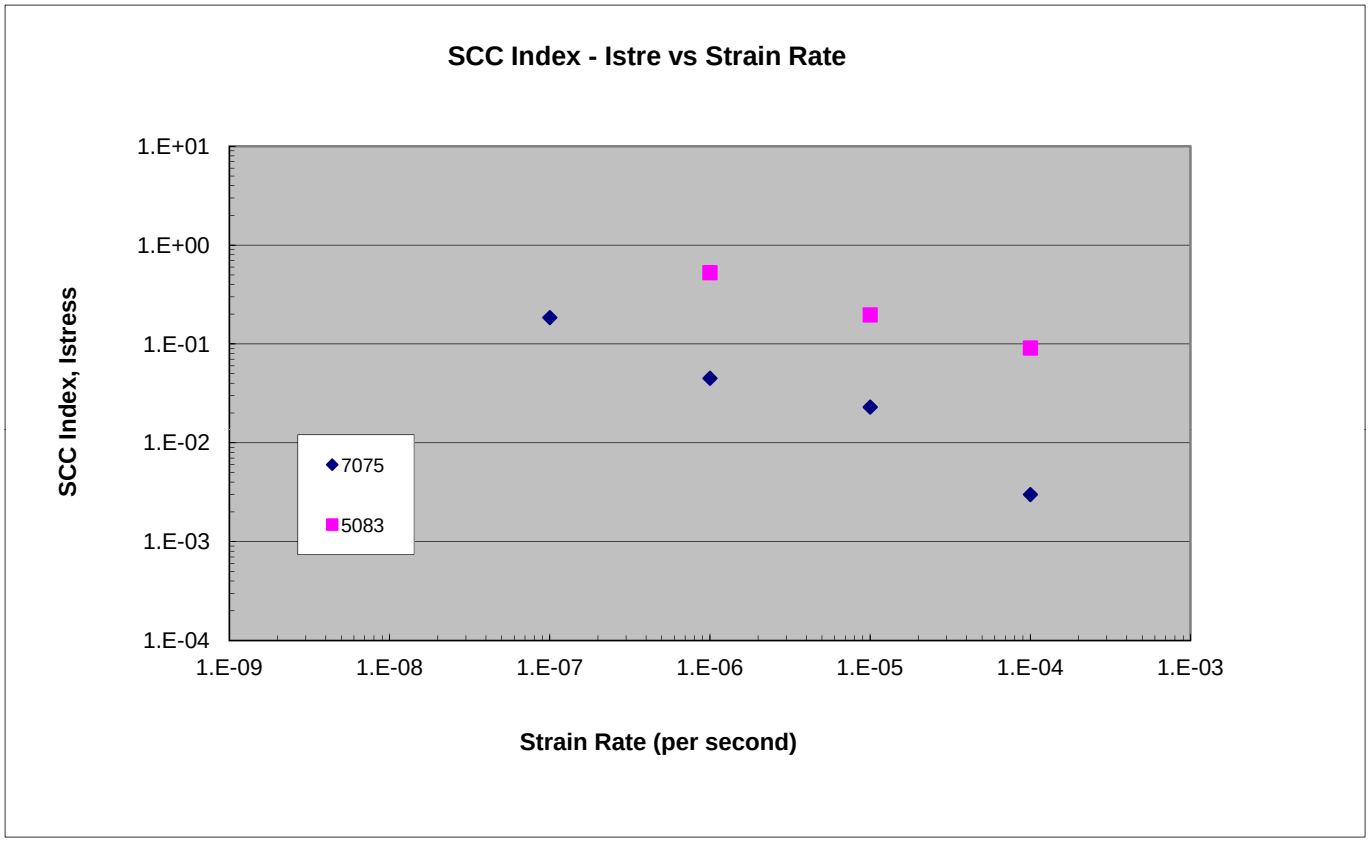

Figure A-11: Variation of SCC Index, I_{stress}, with Strain Rate

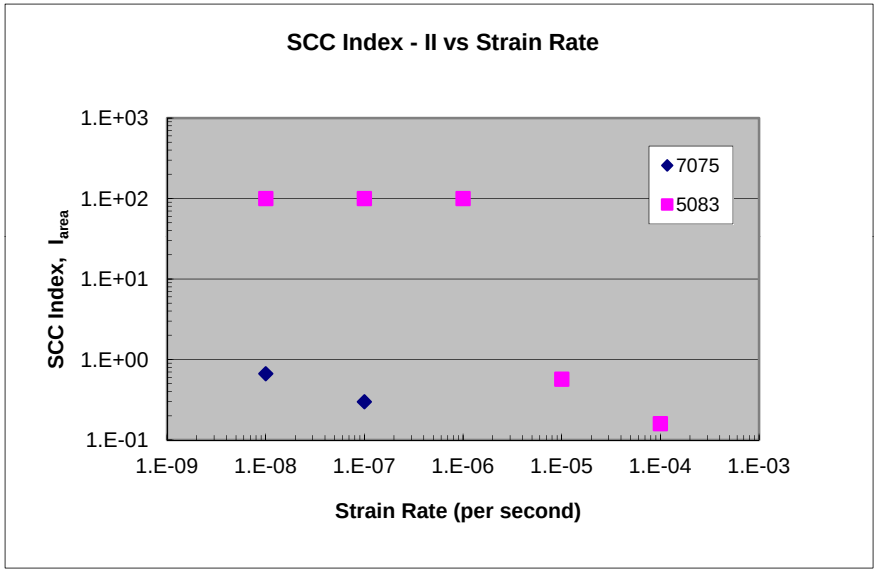

(a)

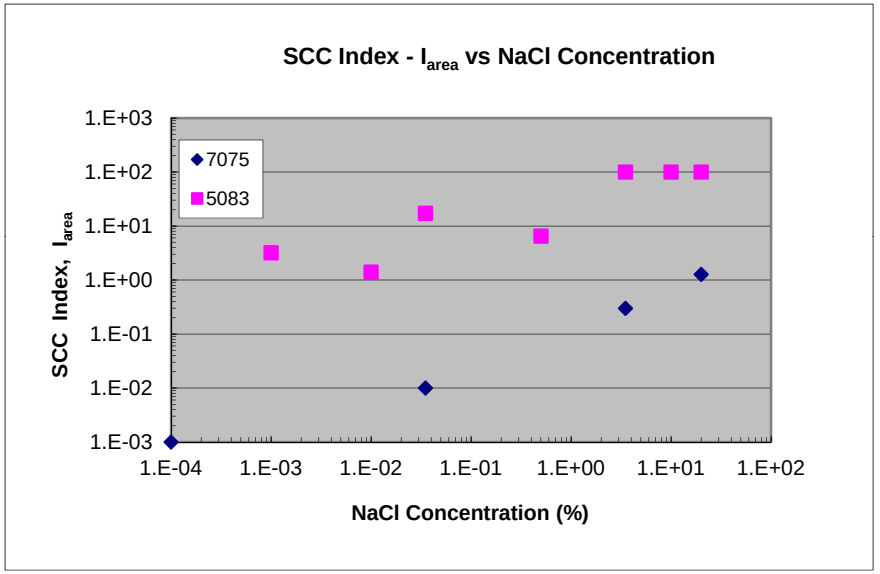

(b)

Figure A-12: Variation of SCC Index, I_{area}, with NaCl Concentration

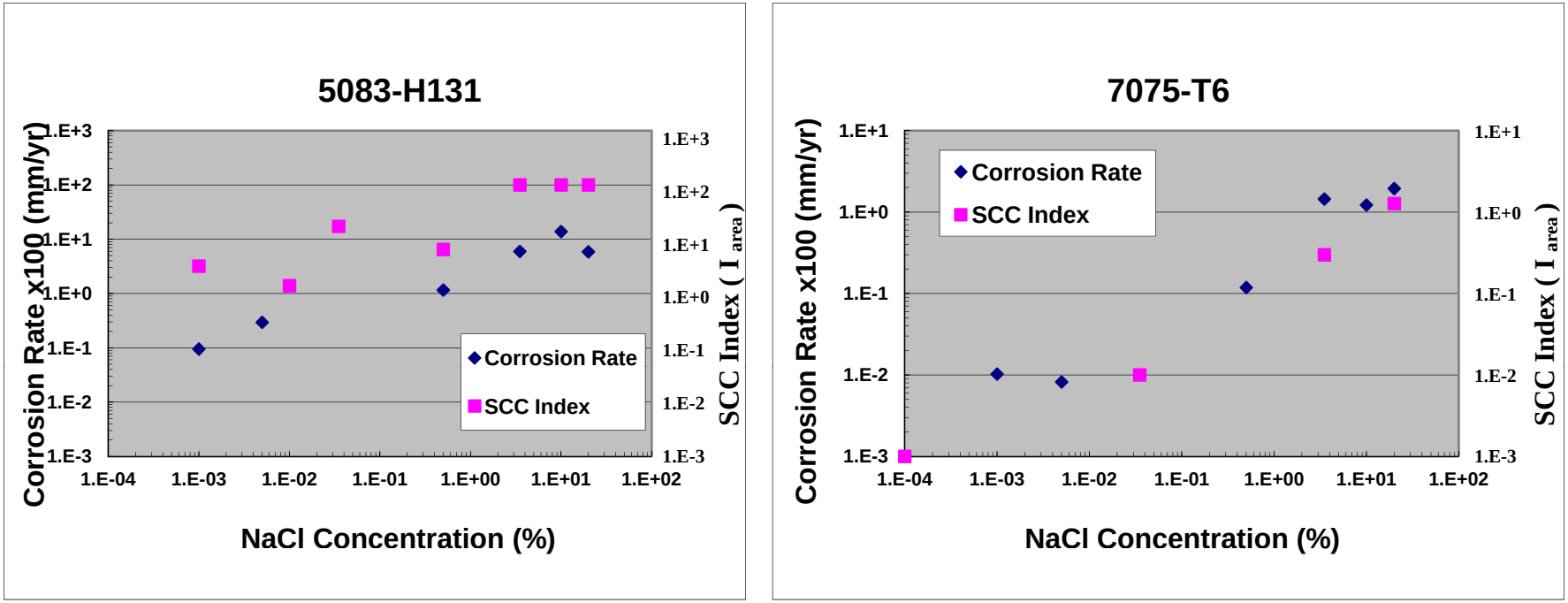

Figure A-13: Variation of Corrosion Rate and SCC Index, I_{area}, with NaCl Concentration for 5083-H131 and 7065-T6 Aluminum Alloys

DISTRIBUTION:

NAVAIRSYSCOM (AIR-4.3), Bldg. 2187, Suite 3340 (1)
48066 Shaw Road, Patuxent River, MD 20670-1906
NAVAIRSYSCOM (AIR-4.3T – Jerry Rubinsky), Bldg. 2187, Suite 3340 (1)
48066 Shaw Road, Patuxent River, MD 20670-1906
NAVAIRSYSCOM (AIR-4.3.4 - Matzdorf), Bldg. 2188 (1)
48066 Shaw Road, Patuxent River, MD 20670-1908
NAVAIRSYSCOM (AIR-4.3.4.1 – Robert Kowalik), Bldg. 2188 (1)
48066 Shaw Road, Patuxent River, MD 20670-1908
NAVAIRSYSCOM (AIR-4.3.4.1 – Eun Lee), Bldg. 2188 (25)
48066 Shaw Road, Patuxent River, MD 20670-1908
FRC/ISSC, Jacksonville, (AIR-4.3.4 - John L. Yadon) (1)
Naval Air Station, Jacksonville, FL 32212
Office of Naval Research, (Code 03R - Dr. Reginald G. Williams) (1)
875 N. Randolph Street, Room 660, Arlington, VA 22203
Office of Naval Research, (Code 332 - Dr. A. K. Vasudevan) (1)
875 N. Randolph Street, Room 629, Arlington, VA 22203
Office of Naval Research, (Code 35 - Mr. William Nickerson) (1)
875 N. Randolph Street, Room 1143B, Arlington, VA 22203
NAVAIRWARCENACDIV (4.12.6.2), Bldg. 407, Room 116 (1)
22269 Cedar Point Road, Patuxent River, MD 20670-1120
DTIC (1)
8725 John J. Kingman Road, Suite 0944, Ft. Belvoir, VA 22060-6218